



**HAL**  
open science

## **A multi-topographical-instrument analysis: the breast implant texture measurement**

Charles Garabédian, Rémi Delille, Raphaël Deltombe, Karine Anselme,  
Michael Atlan, Maxence Bigerelle

► **To cite this version:**

Charles Garabédian, Rémi Delille, Raphaël Deltombe, Karine Anselme, Michael Atlan, et al.. A multi-topographical-instrument analysis: the breast implant texture measurement. *Surface Topography: Metrology and Properties*, 2017, 5 (2), pp.025004. 10.1088/2051-672X/aa7290 . hal-03261666

**HAL Id: hal-03261666**

**<https://hal.science/hal-03261666>**

Submitted on 2 Apr 2024

**HAL** is a multi-disciplinary open access archive for the deposit and dissemination of scientific research documents, whether they are published or not. The documents may come from teaching and research institutions in France or abroad, or from public or private research centers.

L'archive ouverte pluridisciplinaire **HAL**, est destinée au dépôt et à la diffusion de documents scientifiques de niveau recherche, publiés ou non, émanant des établissements d'enseignement et de recherche français ou étrangers, des laboratoires publics ou privés.

# A multi-topographical-instrument analysis: the breast implant texture measurement

Charles Garabédian<sup>1,2</sup>, Rémi Delille<sup>1</sup>, Raphaël Deltombe<sup>1</sup>, Karine Anselme<sup>3</sup> Michael Atlan<sup>4</sup> and Maxence Bigerelle<sup>1</sup>

<sup>1</sup> LAMIH, UMR CNRS 8201, UVHC, Valenciennes, France

<sup>2</sup> Groupe Sebbin SAS, Boissy l'Aillerie, France

<sup>3</sup> IS2M, Mulhouse, France

<sup>4</sup> UPMC Faculté de Médecine, Paris, France

E-mail: [charles.garabedian@laboratoires-sebbin.fr](mailto:charles.garabedian@laboratoires-sebbin.fr)

**Keywords:** breast implant, texturation, roughness

---

## Abstract

Capsular contracture is a major complication after implant-based breast augmentation. To address this tissue reaction, most manufacturers texture the outer breast implant surfaces with calibrated salt grains. However, the analysis of these surfaces on sub-micron scales has been under-studied. This scale range is of interest to understand the future of silicone particles potentially released from the implant surface and the aetiology of newly reported complications, such as Anaplastic Large Cell Lymphoma.

The surface measurements were accomplished by tomography and by two optical devices based on interferometry and on focus variation. The robustness of the measurements was investigated from the tissue scale to the cellular scale.

The macroscopic pore-based structure of the textured implant surfaces is consistently measured by the three instruments. However, the multi-scale analyses start to be discrepant in a scale range between 50  $\mu\text{m}$  and 500  $\mu\text{m}$  characteristic of a finer secondary roughness regardless of the pore shape. The focus variation and the micro-tomography would fail to capture this roughness regime because of a focus-related optical artefact and of step-shaped artefact respectively.

---

## 1. Background

The fifth-generation breast implant outer surface in contact with biological tissues features an irregular texture supposed to stimulate tissue adherence on the implant and subsequently to avoid an anatomical misplacement of the prosthesis [1]. The pore size and pore depth ranges reported by Atlan *et al* [2] are in table 1.

Moreover, more and more clinical evidence is in favor of a texturation on implant surfaces to reduce the capsular contracture occurrence [3]. This complication results from the development of a thick and firm biological layer namely capsule around the implant [4]. Severe capsular contractures are responsible for implant distortion and therefore for patient discomfort, breast pain and poor aesthetic outcome [3].

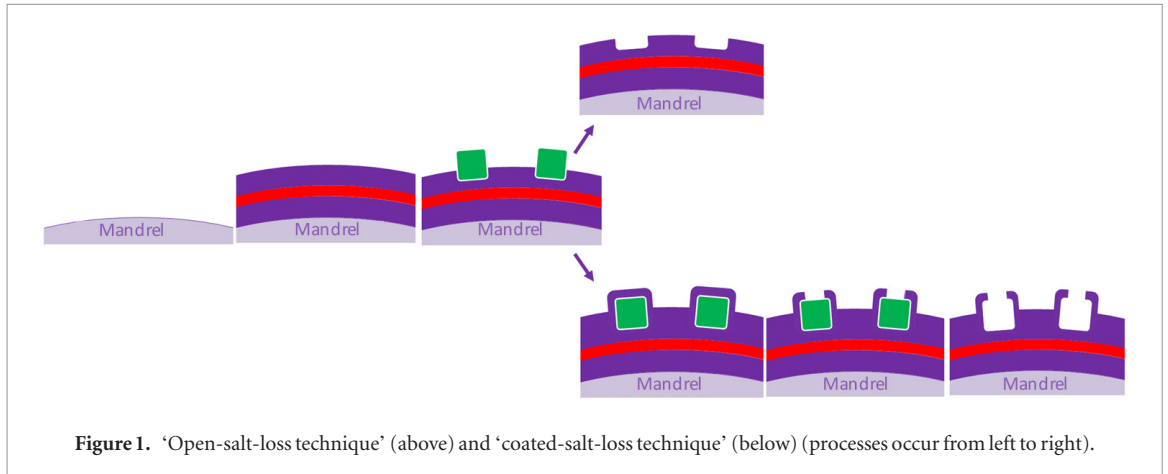
Another complication, namely Breast Implant Associated-Anaplastic Large Cell Lymphoma (BIA-ALCL), draws the attention of sanitary agencies in the

world because the case figures reported by Brody *et al* [5] have sharply increased since 1997. No case of BIA-ALCL has been reported on the Sebbin implants. The aetiology of this cancer type remains purely speculative, however ‘*the fluid associated with ALCL tended to be cloudy and debris filled*’ [5]. Danino *et al* [6] points out the micron-sized silicone particle presence in the capsule. Moreover, other newly reported complications were raised from so-called ‘*macro-textured breast implants*’, such as late seromas or double capsules [7].

According to Whitehouse [8], ‘*all structured surfaces are specifically designed to meet a specific functional requirement*’. For implanted devices, the surface functionality is in term of biological integration. Specific biological entity targeting is the ‘gold-standard’ to promote implant integration. Therefore, interfaces between implanted devices and the host are ideally structured on different length-scale ranges according to the biological targets. For example, the tissue response modulation has to be performed on an approximate

**Table 1.** Pore sizes of two breast implant textures from [2].

	Pore size	Pore depth
Biocell® (Allergan Medical Corporation, Santa Barbara, California)	100–400 $\mu\text{m}$	100–200 $\mu\text{m}$
Sebbin anatomically-shaped implant texture (Boissy l' Aillerie, France)	150–600 $\mu\text{m}$	100–200 $\mu\text{m}$



scale of 300  $\mu\text{m}$ , as reported in the literature relative to bone ingrowth promotion and consequently tissue integration of joint replacement [9]. Conversely, the characteristic scale involved in the sensing of nanometric spatial patterning by molecular mechano-sensors responsible for cell attachment on a substrate is around 3  $\mu\text{m}$  [10, 11].

However, the reported measurement protocols of these interfaces were performed only at the scale of the surface target. A screening of measurement scales between the tissue scales and the cellular scales is understudied in the literature. Regarding breast implant surfaces, this analysis is all the more challenging because of the wide gap between the biological scales. Therefore, in a multi-instrument approach aiming at encompassing the scales from the pore size scale to the silicone particle scale, the accuracy of the measurement instrument will depend on the scale. Only a multi-scale analysis will be of value to compare the robustness between the measurement instruments.

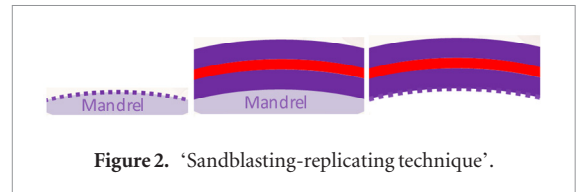
## 2. Materials and methods

### 2.1. Sample preparation

Three Sebbin brand implants featuring three different textures as well as a Sebbin smooth implant were studied.

The Sebbin company uses three processes to texture their implant. The first texturation process based on a salt-loss technique pits the last silicone layers of cuboid pores with calibrated salt crystals. Then the salt is removed in a water bath (figure 1).

Alternatively, the process is extended by covering the silicone surface imprinted of salt with a last silicone layer. After curing, this layer is washed away (figure 1).



Finally, the texturation is also obtained by moulding silicone layers on a sandblasted mandrel (figure 2).

In respect to the International Standard [12] relative to breast implants, three sample sets were peeled from the dome, the radius and the base of the implant shell, each set consisting of three 3 mm-diameter samples. The samples were sonicated in a 10% alcoholic solution during 10 min.

The surface of interest in each sample is the 2 mm-side square inside the circular sample.

### 2.2. Surface characterizations

To encompass a large wavelength range, measurements were performed with x-ray micro-tomography (Skyscan™ 1172, Bruker, Billerica, USA), two optical devices, namely the White-Light Interferometer (NewView™ 7300, Zygo, Middlefield, USA) and a Focus variation microscope (Infinite Focus™, Alicona Imaging GmbH, Grambach, Austria) and a Field Emission Gun-Scanning Electronic Microscope (JEOL 7100F TTLS, Tokyo, Japan).

#### 2.2.1. X-ray micro-tomography.

The micro-tomography scan is a Skyscan™ 1172 with a resolution of 2.50  $\mu\text{m}$  and a x-ray source at 80 kV and 100  $\mu\text{A}$ . The scans are imaged on a 4K  $\times$  2K pixel CCD camera

The reconstruction of scans to a stack of cross-sections along the  $z$ -axis was performed after filtering

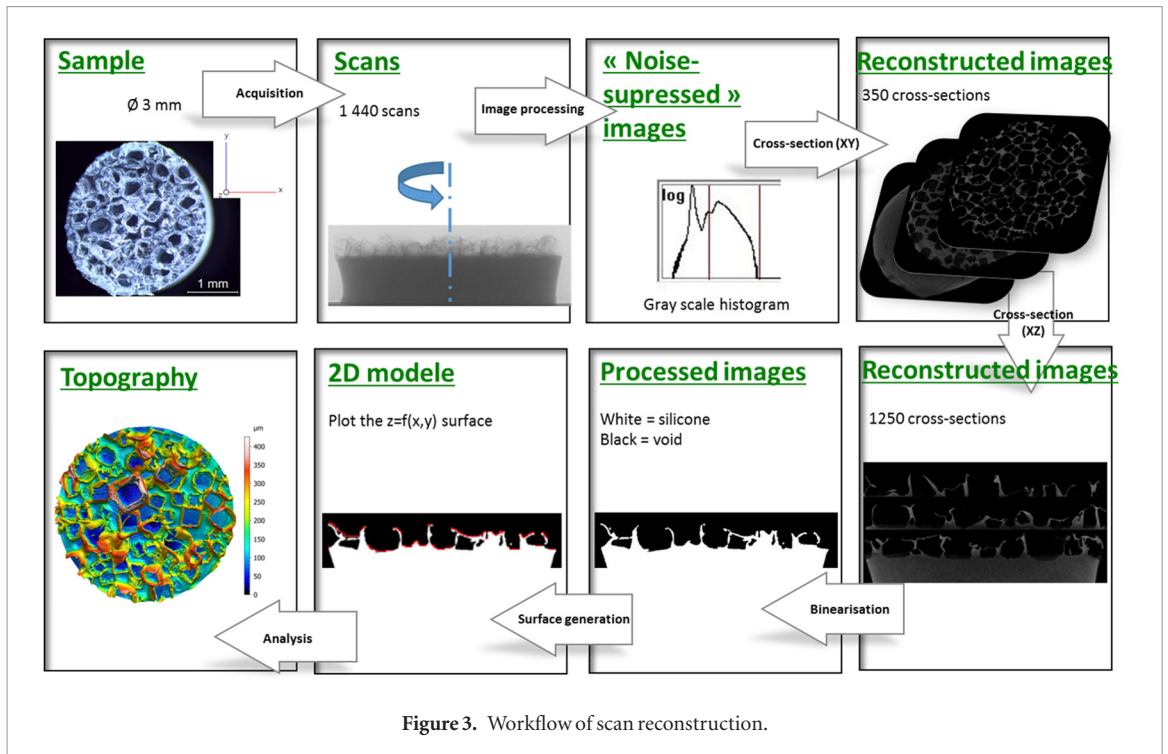


Figure 3. Workflow of scan reconstruction.

Table 2. Optical settings of White-Light Interferometer and Alicona Infinite Focus™ microscope.

Measured surfaces	Interferometry		Focus variation	
	Textured implant surface	Smooth implant surface	Salt-based textured implant surface	Sandblasted-replicated and smooth implant surface
Objective	50×	100×	10×	50×
Vertical resolution	10 nm	10 nm	1 µm	210 nm
Lateral resolution	0.52 µm	0.32 µm	6.52 µm	4 µm

the noise peak. This stack is converted to a file of cross-sections in the  $(xy)$  plane. After binarization of the cross-sections, the topography is obtained by capturing the most outer point for each  $(x, y)$  position in a matrix (figure 3).

### 2.2.2. White-Light Interferometer and Alicona Infinite Focus™ microscope.

The interferogram bucket is imaged on each pixel of a black and white  $640 \times 480$  pixel CCD camera. Each individual surface is gathered according to the stitching method [13]. The stitching matrix of interferograms consists of  $15 \times 20$  images and the overlapping is 20%. To measure all the textures, the scan length of the electric Z-device has to be extended as high as  $800 \mu\text{m}$ .

The focus variation was computed under a ring light source.

For the two instruments, the choice of the objective and the resulting lateral and vertical resolutions are summarized in the table 2 according to the texture type.

### 2.2.3. Field Emission Gun-Scanning Electronic Microscope (FEG-SEM).

The samples were pinned to the stage. The acceleration voltage is 1 kV and the working distance is approximately 15 mm.

## 3. Results

### 3.1. Surface topographies

The texture morphologies measured by the three instruments are similar (figures 4). Remarkably, sub-micrometric smooth droplets seem to spread on the smooth implant surface (figure 4(A)). The salt-based topographies exhibit randomly-arranged cuboid depressions. The open pores walls are thinner and higher in the ‘coated-salt-loss texture’ than in the ‘open-salt-loss texture’ (figures 4(B) and (C)). Many random peaks of maximal  $100 \mu\text{m}$  height feature the ‘sandblasting-replicating texture’ (figure 4(D)).

In respect to the International Standard [12], Scanning Electronic Microscope (SEM) images were also performed to capture the three textures (figure 5).

### 3.2. Multi-scale analysis

In this study, all surfaces were flattened by a third degree polynomial fit to remove the form of the surface (Mountains Digital Surf™, Besançon, France). No post-measurement sampling and no refilling procedure was applied.

By applying High-Pass filters of lower and lower cut-off wavelengths to the surface, finer and finer

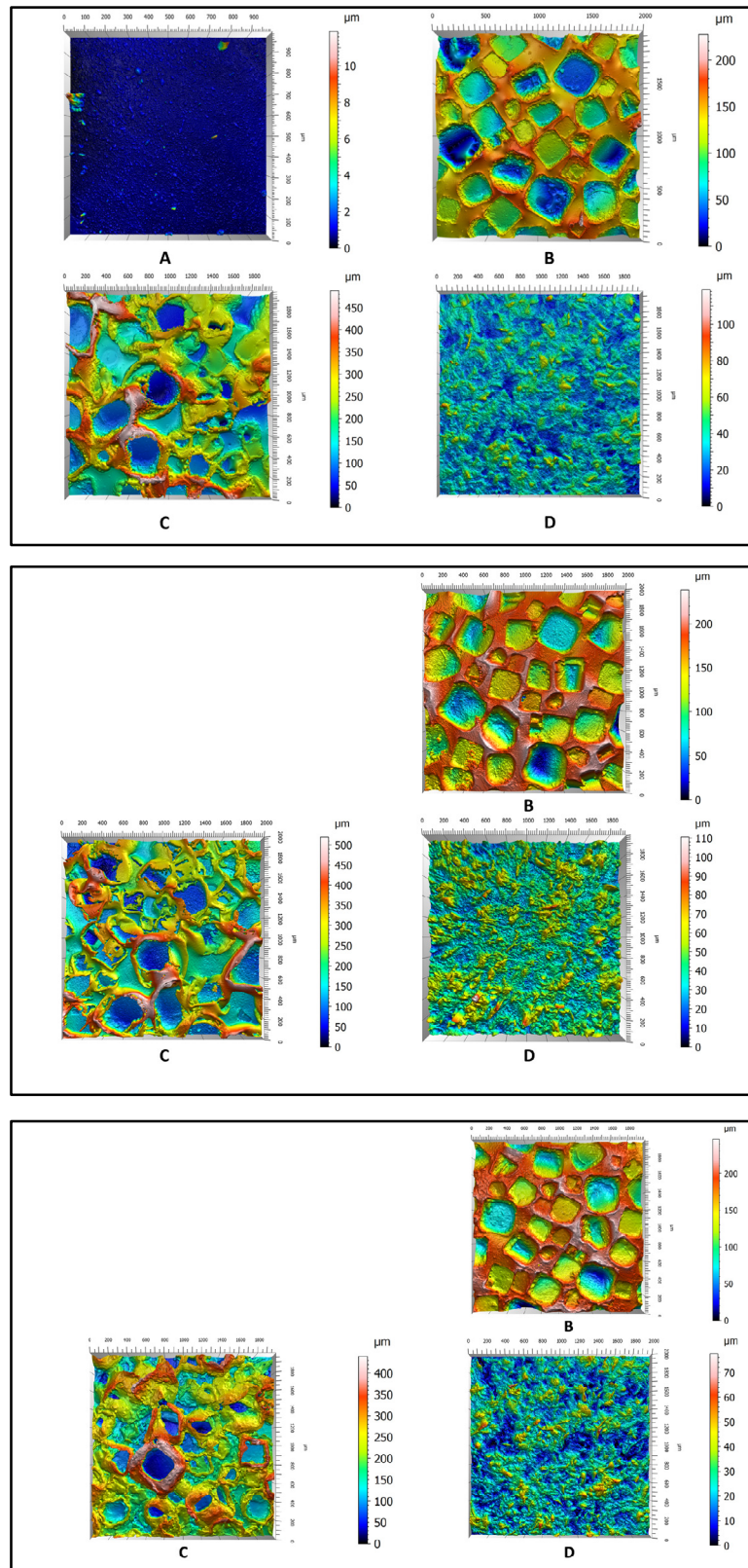


**Figure 4.** Topographies of the Sebbin smooth implant (A) and the three Sebbin textures (the ‘open-salt-loss texture’ (B), the ‘coated-salt-loss texture’ (C) and the ‘sandblasting-replicating texture’ (D)) measured by interferometry (first panel), by micro-tomography (second panel) and by Focus variation (third panel).

roughness is isolated from the surface and smaller and smaller scales are therefore captured. Firstly, the 3D arithmetic mean height ( $S_a$ ) was computed on each filtered surface. This processing was implemented on the set of nine surfaces measured at different locations on

the prosthesis, resulting in the below multi-scale curves (figure 6).

The  $S_a$  was retained as a first parameter for the multi-scale analysis, from which an insight on the frequential content of the surface can be drawn.

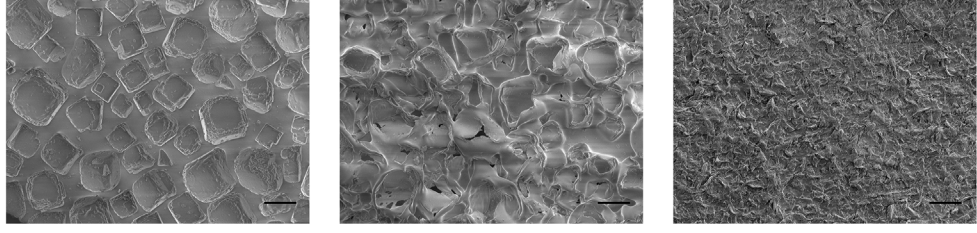


**Figure 5.** The ‘open-salt-loss technique’, the ‘coated-salt-loss technique’ and the ‘sandblasting-replicating technique’ (from left to right). Magnification 40×. Scale bar: 100  $\mu\text{m}$ .

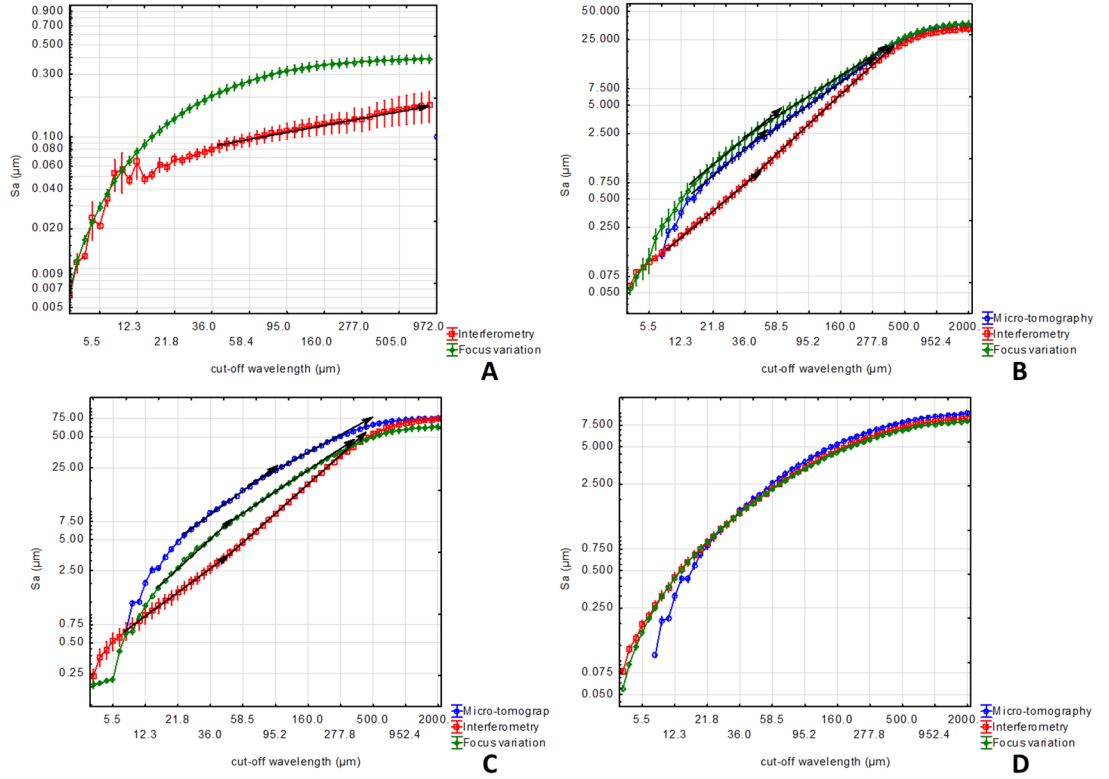


**Figure 6.** Sa high-pass multi-scale decompositions of the smooth implant surface (A), the ‘open-salt-loss texture’ (B), the ‘coated-salt-loss texture’ (C) and the ‘sandblasting-replicating texture’ (D). The linear tendencies are pointed out by black arrows.

### 3.2.1. Smooth implant surfaces.

A linear evolution—the hallmark of fractal regime—characterizes the curve measured on the smooth implant surface by Interferometer on scales superior to 40  $\mu\text{m}$  (figure 6(A)). If the linear slope is mentioned  $H$  (Hurst exponent), the fractal dimension is then given by (1).

$$\Delta = 2 - H \quad (1)$$

Practically, a fractal surface exhibits the same pattern on several scales. The figure 7(A) highlights the wide range of droplet sizes on the smooth implant surface measured by interferometry microscope, contrary to the one measured by Focus variation (figure 7(B)).

Fractal structures are expected to maintain their height-diameter ratio over length scales. Wolf pruning method [14] was implemented on all filtered smooth implant surfaces with screening of minimal height motif, ranging from 0.1% to 10% of the maximal peak height ( $S_z$ ). If the peak height of each motif is plotted

in function of the peak equivalent diameter in log–log scale (figure 8), the peak fractal dimension is determined as previously (1) with the slope  $H$  [15].

As highlighted in the figure 8, both curves exhibit three behaviours:

The first stage features the scales inferior to 22  $\mu\text{m}$  and 14  $\mu\text{m}$ , as shown respectively by the Focus variation-related curve and the Interferometry-related curve. The fractal dimension is equal to 2. Under this threshold, topographical instruments fail to measure topography. At this small scale, the output signal from the instrument is a noise. Subsequently, the watershed algorithm results in a noise discretization. Moreover, by considering these thresholds as the instrument lateral resolutions, the Focus variation lateral resolution is approximately twice less precise than the Interferometry one (22  $\mu\text{m}$  and 14  $\mu\text{m}$  respectively). Remarkably, this ratio is consistent with the apparatus settings since the surface is imaged with a 100× and a 50× objective, respec-

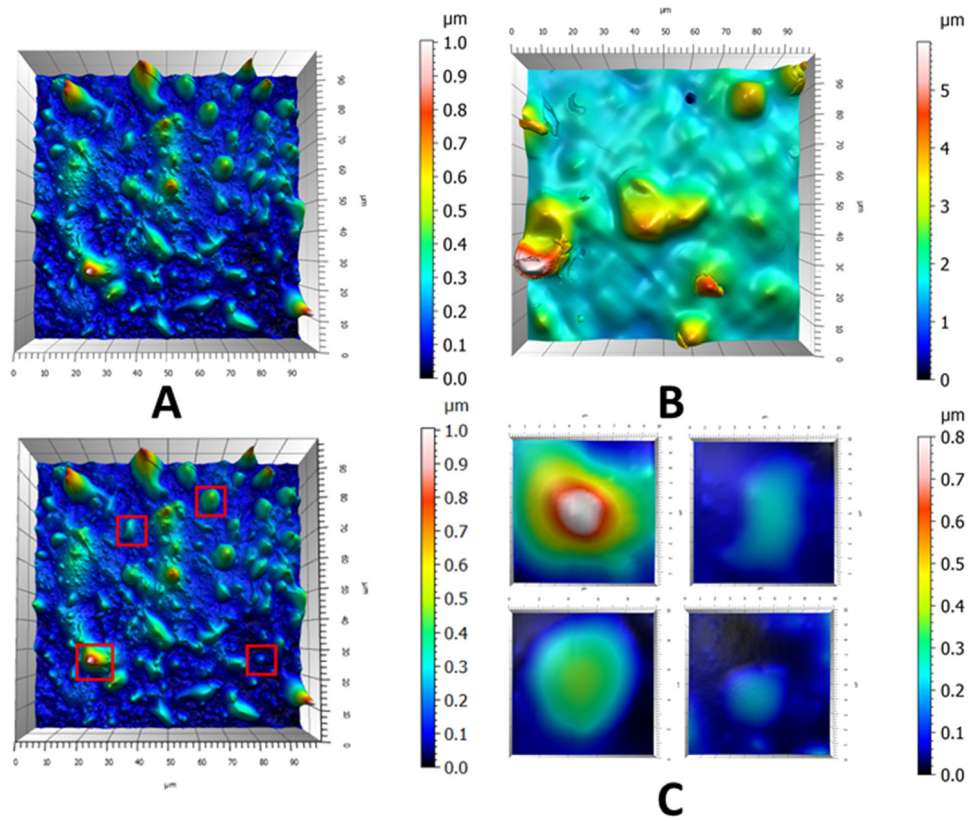


**Figure 7.** Smooth implant surfaces measured by Interferometer (A) and by Focus variation (B). Samples from the fractal droplet size distribution on the Interferometer-measured smooth implant surface (C).

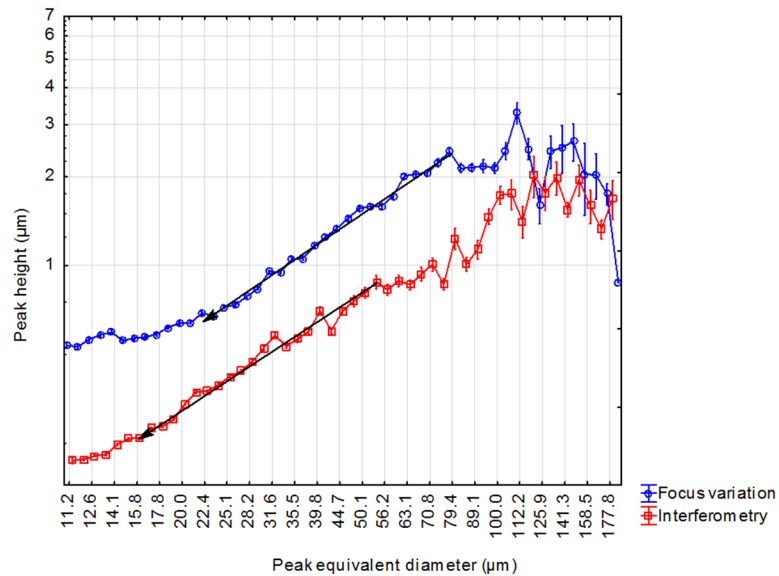


**Figure 8.** Peak ranking of the smooth breast implant surface according to peak height and to peak equivalent diameter. Black arrows highlight homothetic peak regimes.

tively in Interferometry and in Focus variation, resulting in the respective finest lateral resolutions  $0.32 \mu\text{m}$  and  $0.64 \mu\text{m}$ .

The second stage ranges from  $22 \mu\text{m}$  to  $80 \mu\text{m}$  and from  $14 \mu\text{m}$  to  $50 \mu\text{m}$ , respectively for the Focus variation and the Interferometry. Both curves exhibit a slope equal to 1. As a result, peak shapes are Euclidian and not fractal. Practically, a range of homothetic

peaks was measured by Interferometer and by Focus variation over these scales. Interestingly, the Focus variation measurement shifts this range to 100% upward in height and to 20% upward in diameter. The over-estimation of the peak size resulting from the Focus variation measurement might be an optical artefact. By diffusing extensively light, silicone would enlarge the focus in height and in diameter compared to the real

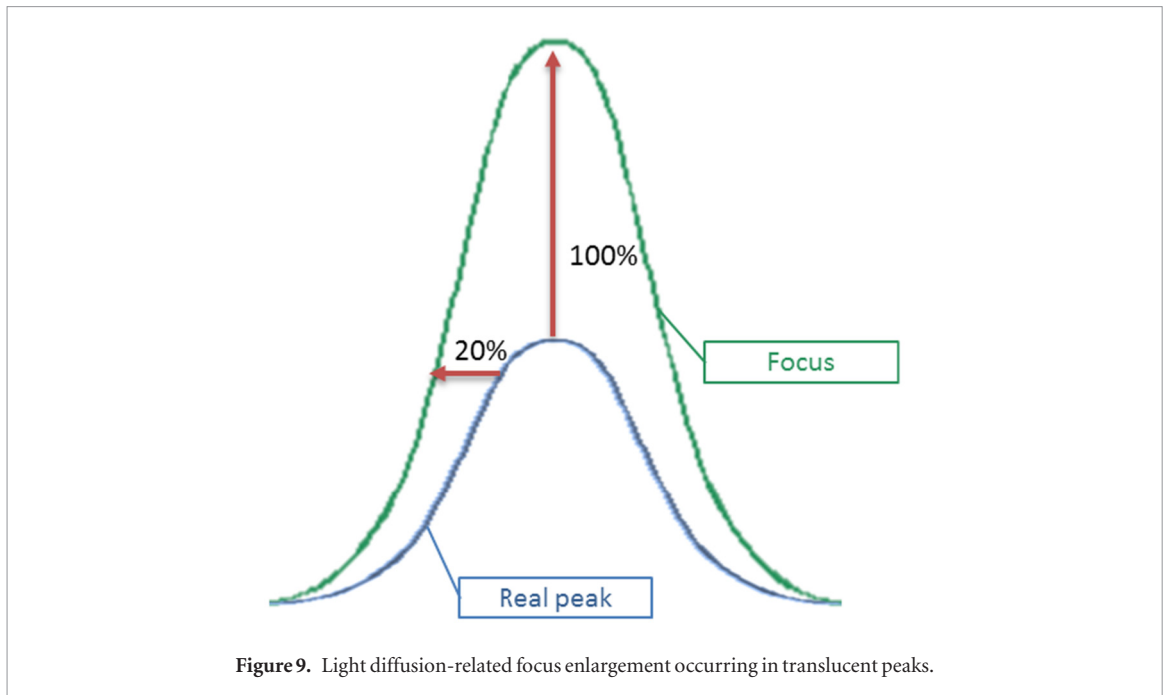


**Figure 9.** Light diffusion-related focus enlargement occurring in translucent peaks.

**Table 3.** Multi-scale parameters characteristic of the salt-based textured surfaces.

		‘Open-salt-loss texture’		‘Coated-salt-loss texture’	
		Hurst exponent	Lower boundary ( $\mu\text{m}$ )	Hurst exponent	Lower boundary ( $\mu\text{m}$ )
Interferometry	Second regime	0.052	35.594	0.124	45.512
	Third regime	0.023	10.593	0.075	9.762
Micro-tomography	Second regime	0.061	47.992	0.175	73.619
	Third regime	0.059	19.794	0.263	26.592
Focus variation	Second regime	0.066	40.824	0.146	46.626
	Third regime	0.074	21.669	0.173	16.004

peak (figure 9). Consequently, focalisation technique may fail to capture some translucent peaks.

The Focus variation and the Interferometry measurements start the third stage from  $80 \mu\text{m}$  and from  $50 \mu\text{m}$  respectively. The slope almost equal to zero means that peak heights remain approximately constant whatever the motif size. Therefore, the roughness correlation is completed.

### 3.2.2. Salt-based textured surfaces.

The multi-scale analyses of the ‘open-salt-loss texturation’ (figure 6(B)) and the ‘coated-salt-loss texturation’ (figure 6(C)) feature for each instrument 3 regimes. The Hurst exponent and the wavelength boundary values are reported for each regime in table 3.

The first stage includes scales superior to approximately  $500 \mu\text{m}$ . This stationary regime is the hallmark of the macroscopic pores pitted by salt grains. As illustrated in the previously mentioned figures, the resulting measurements from the three instruments are robust to capture the salt-related macroscopic topography. This robustness between the instruments is all the more valuable as interferometric measurement captures a very reduced number of points on full sharp slopes.

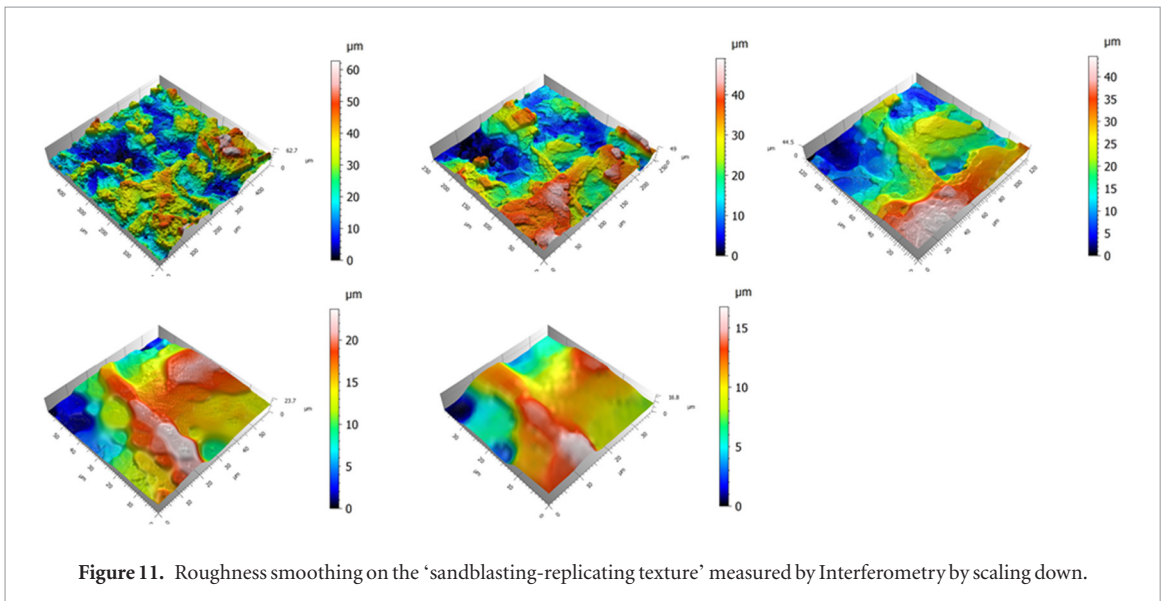
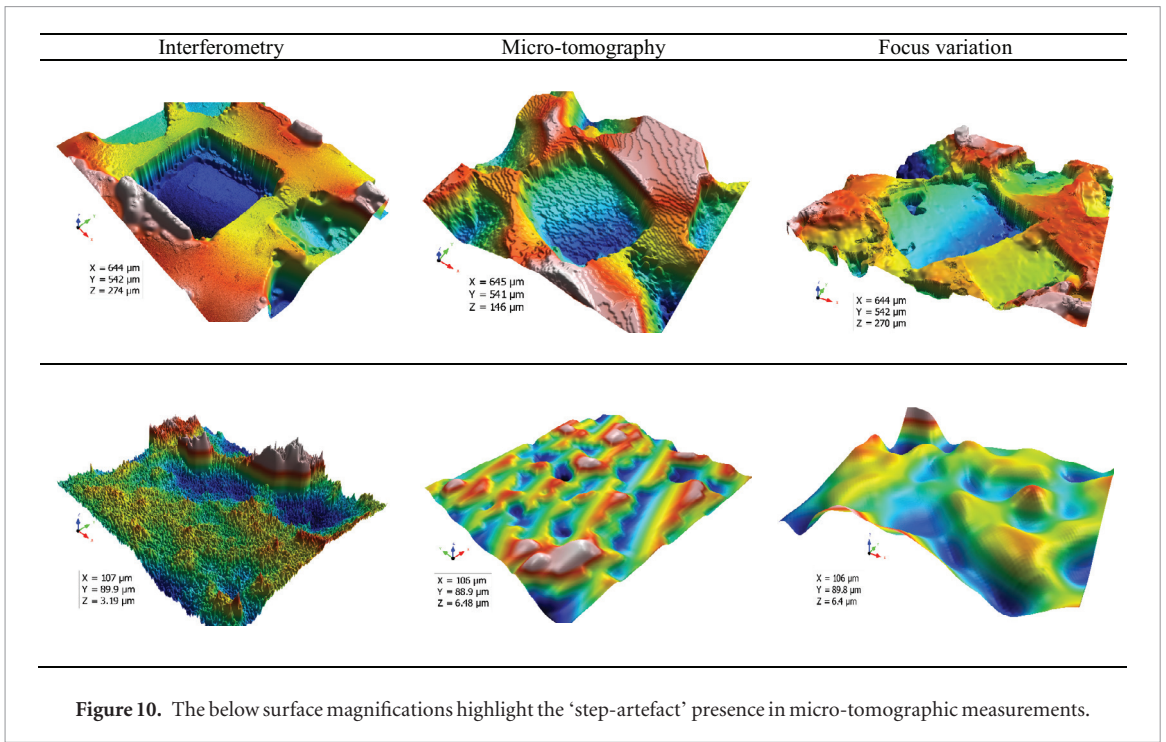
The second stage is characteristic of scales between  $50 \mu\text{m}$  and  $500 \mu\text{m}$ . Over these scales, roughness on

the bridging areas between the pits and on the bases of depressions is responsible for these fractal regimes. These surface features consist of silicone waviness and deformation and discrepancy in salt pitting depth. Interestingly, the  $S_a$  values are higher in the micro-tomography- and in the Focus variation-related curves than in the interferometric one. The small steps paving the micro-tomography-measured surfaces (figure 10) and the peak enlargement caused by a higher resolution in the Focus variation measurements, as mentioned previously, may be responsible for these higher  $S_a$  values.

The lower boundaries of the third stage are mentioned in the table 3 and represent the apparatus lateral resolutions. Therefore, once again the micro-tomography and the Focus variation lateral resolutions are much higher than the Interferometry one. These fractal regimes encompass the intrinsic elastomer roughness, regardless of grain shape.

### 3.2.3. ‘Sandblasted-replicated surfaces’.

Surprisingly, no scaling law is identified on the ‘sandblasting-replicating texturation’-related curves (figure 6(D)), although stochastic processes, like sandblasting, are the ‘gold-standard’ to manufacture a multi-scale surface. All sandblasting scales may not be imprinted on



the silicone replica (figure 11), resulting in roughness smoothing on the smallest scales.

### 3.3. Extension to other parameters

To refine the topographical characterization of such surfaces, a similar multi-scale procedure was implemented on four other height parameters: the root mean square height (Sq), the maximal height (Sz), the kurtosis (Sku) and the skewness (Ssk).

A linear correlation was established between the Sa and the Sq (figure 12) with a factor of 0.8. The factor was theoretically demonstrated on the 2D parameters [16]:

$$Ra = Rq \sqrt{\frac{2}{\pi}} \approx 0.8Rq. \quad (2)$$

The Sa and the Sz are also correlated (figure 12). Therefore, the approach led on the Sa may be easily extrapolated for the Sq and the Sz.

The multi-scale curves are in the figures 13 and 14 for the Sku and the Ssk respectively.

A scaling down of the smooth surface measured by Interferometer exhibits a decreasing Sku and Ssk to a length scale of 12  $\mu\text{m}$  (figures 13(A) and 14(A)). Basically, the smooth surface features a range of isolated peaks. When the large scales are filtered, the highest peaks are less and less sharp (figure 15). Therefore, the Sku is expected to decrease during the filtering.

Moreover, the surface is more and more symmetrical because the peaks are less and less high, hence a reduction of the Ssk. Below the scale of 12  $\mu\text{m}$ , the increases of the Sku and the Ssk are characteristic of the droplets described previously with a size range between 10  $\mu\text{m}$  and 50  $\mu\text{m}$  (figure 7). The Focus variation curves support the mentioned tendencies. However, the optical artefact of the focus is responsible for a downward shift of the values. Basically, as the peak base is wider, the Sku is lower.

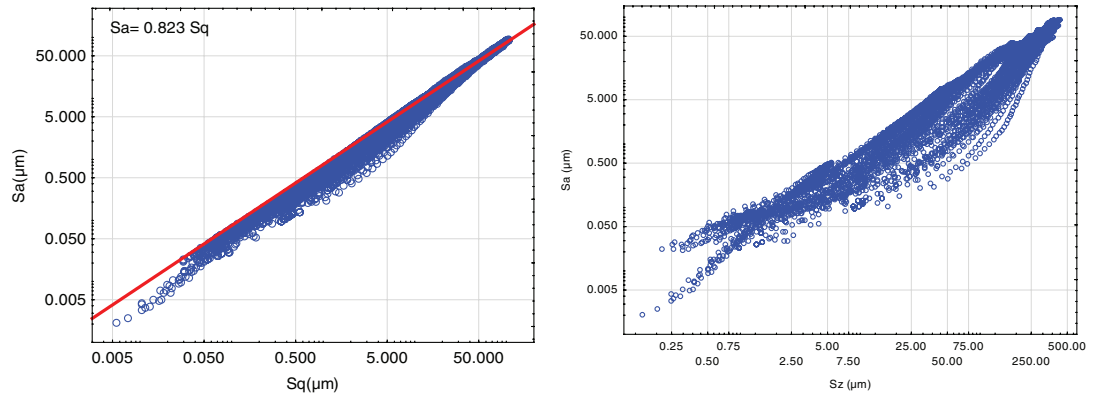


Figure 12. Correlation between the Sa and the Sq and between the Sa and the Sz.

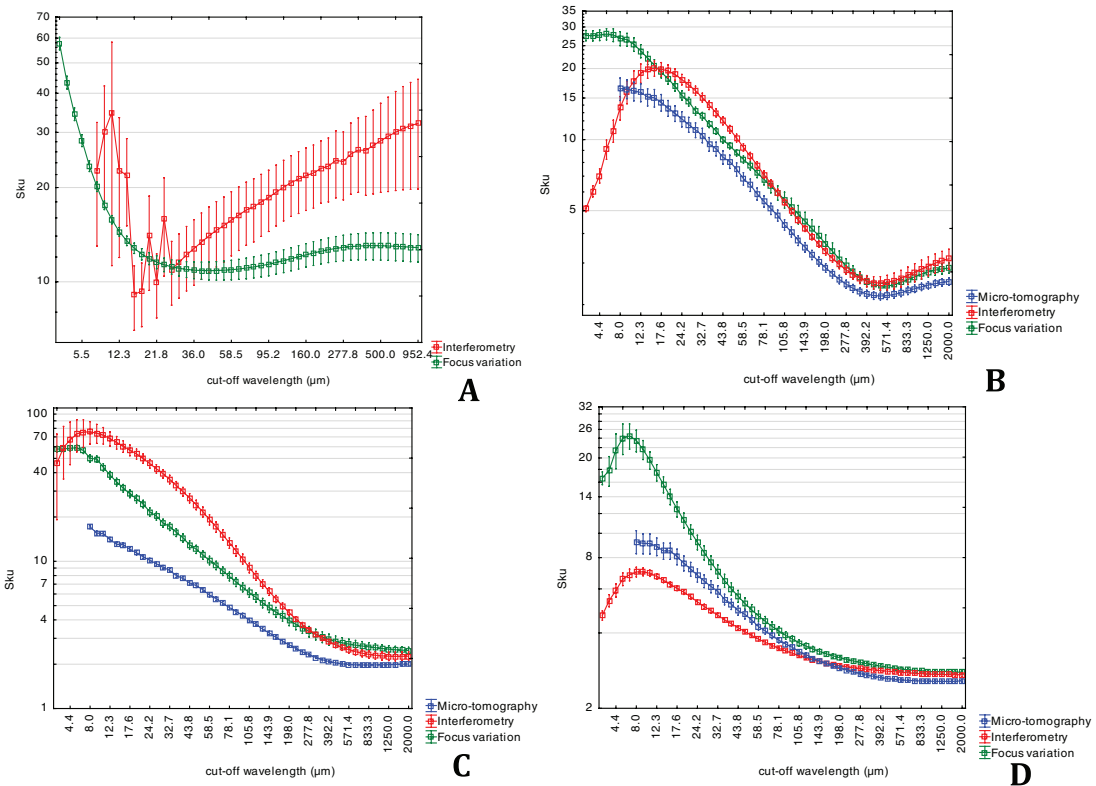


Figure 13. Sku high-pass multi-scale decompositions of the smooth implant surface (A), the ‘open-salt-loss texture’ (B), the ‘coated-salt-loss texture’ (C) and the ‘sandblasting-replicating texture’ (D).

For the two salt-based textured surfaces, the multi-scale curves of the Sku are similar for the three instruments (figures 13(B) and(C)). The scale range above 500  $\mu\text{m}$  captures the pore regime. Then the Sku increases between 500  $\mu\text{m}$  and 10  $\mu\text{m}$ . Below the pore scale, a massif of peaks appears at the boundaries of the pores. These peaks are more and more spiked during the filtering (figure 16). Therefore, the Sku is expected to increase. A decrease of the Sku for the Interferometry occurs at the detection limit measured on the multi-scale curve of the Sa (figure 6).

Regarding the Ssk curves of the salt-based textured surfaces (figures 14(B) and (C)) the Micro-tomography and the Focus variation measure an approximate

symmetrical surface at every scale with a Ssk close to 0. The reference plane is therefore translated upward. The Interferometer exhibits a significant increase of the Ssk at the small scales, characteristic of some silicone pore walls abraded during the manufacturing process (figure 17). The Ssk of the ‘coated-salt-loss texture’ is therefore consistently higher than the Ssk of the ‘open-salt-loss texture’.

As the sandblasted surface exhibits an increasing Sku (figure 13(D)), the peaks are sharper and sharper at the small sandblasting scales. Moreover, whatever the scale and the instrument, the surface is symmetrical, as proven by the small discrepancies in the Ssk values (figure 14(D)).

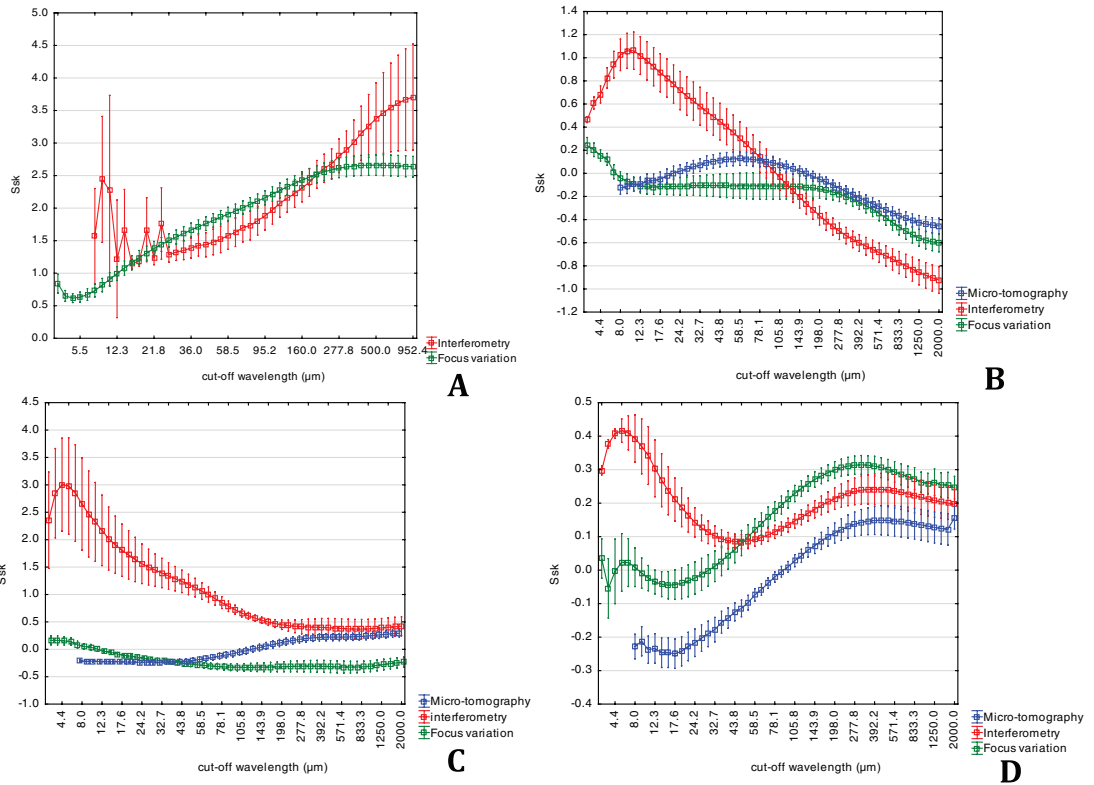


**Figure 14.** Ssk high-pass multi-scale decompositions of the smooth implant surface (A), the ‘open-salt-loss texture’ (B), the ‘coated-salt-loss texture’ (C) and the ‘sandblasting-replicating texture’ (D).

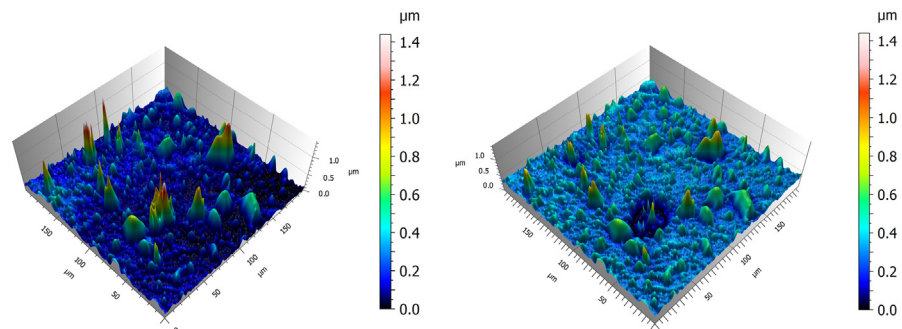


**Figure 15.** Blunting of the peaks on the smooth surface at small scales. The right picture is filtered with a cut-off of 36 μm.

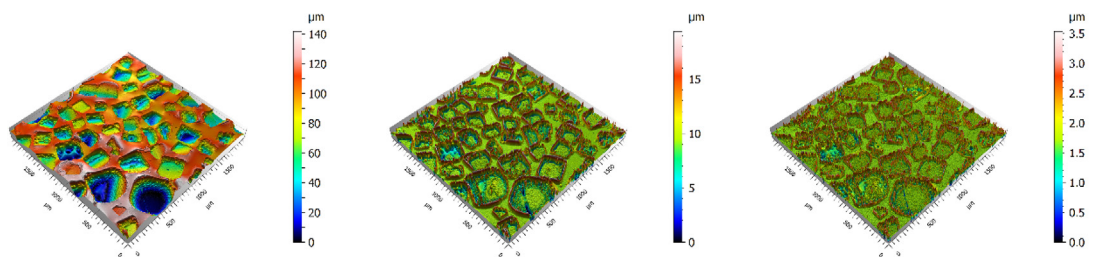


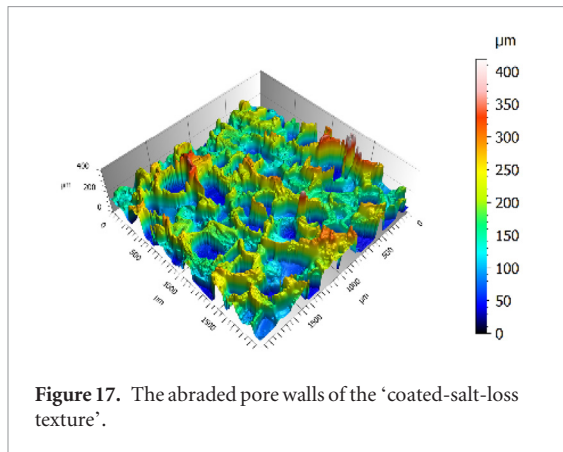
**Figure 16.** Spiking of the peak regime on the salt-based textured surfaces. The middle and the right pictures are filtered with a cut-off of 53 μm and 20 μm respectively.

#### 4. Discussion

No extensive and comparative topographical analysis was performed on breast implant shells. Only preliminary surface measurements prior to biological characterizations were reported in the literature [17, 18].

Moreover, the current International Standard relative to breast implants [12] is elusive about the metrological material requirements.

This multi-instrument and multi-scale analysis highlights valuable metrological methodology and results for the editing of a breast implant texture



measurement procedure. This study is focused on three instruments: x-ray micro-tomography, White-Light Interferometry and Focus variation microscopy. However, the methodology which aims at comparing the instrument accuracies over a wide scale range encompassing the tissue and the cellular scales is easily extrapolated to other apparatus, such as laser confocal microscopy and atomic force microscopy (AFM).

In spite of an important non-measured point number on full sharp slopes, the White-Light Interferometer is the instrument which has the most complete insight into Sebbin textured breast implant surface topography. Three roughness regimes feature its multi-scale analysis: the pore-based macroscopic structure and two fractal regimes characteristic of secondary salt-derived roughness and of intrinsic silicone roughness. Moreover, contrary to Focus variation, Interferometry captures the fractal sub-micrometric droplets present on Sebbin smooth implant surface.

Usually computer-tomography (CT) is the ‘gold-standard’ of volumic measurement, especially of porosity computation [19]. Remarkably, the macroscopic topography resulting from the  $\mu$ -CT measurement and from the downstream reconstruction procedure is robust and metrologically of value. Sebbin textures have been already measured by x-ray micro-tomography without topographical analysis [2]. The texturation scale is also consistent with the calibration specification of the manufacturer. However, a 20  $\mu\text{m}$ -wide ‘step-artefact’ occurring all over the surface would overestimate the secondary roughness.

The Focus variation accurately captures the primary salt-based roughness. Yet, its measuring principle must be questioned for investigating sub-micrometric translucent features. The light reflection off the surface and the computation of a non-coherent light property—the focus—would result in a non-isotropic artefact led to a 100% motif height increase and a 20% motif diameter increase in Sebbin smooth implant surface and in a higher secondary roughness than the interferometric measurements in Sebbin textured implant surface. This focus enlargement could hinder the measurement of small surface roughness on uncharged-silicone replica.

The multi-scale analysis performed on the ‘sandblasting-replicating surfaces’ is not conclusive because of some silicone-replicating-related artefacts. The smallest sandblasting scales are blanked out on the silicone replica because the silicone gel used does not bridge the smallest mandrel roughness. A surface analysis of the mandrel will interestingly complete the results.

According to the multi-scale curves, the three measuring protocols are robust in the capture of the Sebbin textured breast implant macro-structures. Breast implants of other manufacturers were macroscopically investigated in the literature. Valencia-Lazcano *et al* [17] measured on an Allergan Biocell<sup>®</sup> implant a couple of topographical parameters on a  $644 \times 642 \mu\text{m}$  square, contrary to the International Standard requirements [12]. However, the reported Sa value ( $Sa = 18.83 \pm 0.91 \mu\text{m}$ ) [17] is widely underestimated because measuring pores with a largest size of 522  $\mu\text{m}$  over an area of approximate  $640 \mu\text{m}^2$  is topographically irrelevant.

Valencia-Lazcano *et al* [17] and Kyle *et al* [18], both from the University of Manchester, also performed a surface analysis on a Mentor Siltex<sup>®</sup> implant (Mentor Corporation, Santa Barbara, California). A significant discrepancy in the maximal height of the surface (328  $\mu\text{m}$  and 40  $\mu\text{m}$ , respectively from [17, 18]) questions their measuring protocols and their samplings.

The secondary roughness regime is the first discriminating scale range between the three instruments. Barr *et al* [20] paved the way of a multi-scale analysis with a SEM image set capturing the Allergan Biocell<sup>®</sup> texturation over a surface size range from  $2.5 \times 2.0 \text{ mm}$  to  $27.8 \times 37.5 \mu\text{m}$ . At the highest magnifications, Barr *et al* exhibits the ‘lack of surface characteristics’ between the pores and a ‘finer wavy topography to its internal surface’, which would be the hallmark of this secondary roughness regime.

Smooth Sebbin implant and smooth Mentor implant [18] surfaces feature random nano- and micro-scale peaks, contrary to ripples characteristic of smooth Allergan implant surfaces [20]. Different polymer curing processes may be responsible for these two patterns.

## 5. Conclusion

The White Light Interferometer captures the widest topographical content of the textured breast implant surfaces over the largest scale range (from the pore size to the scale of 10 nm). To improve the breast implant integration, which is a multi-scale challenge from the tissue scale to the cellular sensor scale, a measurement of the textures by Interferometer is the ‘gold standard’, compared to the Micro-tomography and the Focus variation.

## References

- [1] Maxwell G P, Scheffan M, Spear S, Nava M B and Hedén P 2014 *Aesthetic Surg. J.* **34** 876–81
- [2] Atlan M, Bigerelle M, Larreta-Garde V, Hindié M and Hedén P 2016 *Aesthetic Plast. Surg.* **40** 89–97
- [3] Barnsley G P, Sigurdson L J and Barnsley S E 2006 *Plast. Reconstr. Surg.* **117** 2182–90

- [4] Barr S and Bayat A 2011 *Aesthetic Surg. J.* **31** 56–67
- [5] Brody G S, Deapen D, Taylor C R, Pinter-Brown L, House-Lightner S R, Andersen J S, Carlson G, Lechner M G and Epstein A L 2015 *Plast. Reconstr. Surg.* **135** 695–705
- [6] Danino A M, Basmacioglu P, Saito S, Rocher F, Blanchet-Bardon C, Revol M and Servant J M 2001 *Plast. Reconstr. Surg.* **108** 2047–52
- [7] Hall-Findlay E J 2011 *Plast. Reconstr. Surg.* **127** 56–66
- [8] Whitehouse D J 2010 *Handbook of Surface and Nanometrology* 2nd edn (Boca Raton, FL: CRC Press)
- [9] Kujala S, Ryhänen J, Danilov A and Tuukkanen J 2003 *Biomaterials* **24** 4691–7
- [10] Stevenson P M and Donald A M 2009 *Langmuir* **25** 367–76
- [11] Li F, Li B, Wang Q M and Wang J M 2008 *Cell. Motil. Cytoskeleton* **65** 332–41
- [12] ISO 14607 2009 Non-active surgical implants—mammary implants—particular requirements (Bruxelles European Committee for Standardization)
- [13] Roth J and de Groot P 1997 *Proc. of ASPE Spring Topical Meeting on Advances in Surface Metrology (Annapolis, MD)* pp 57–60
- [14] Scott P J 2004 *Proc. R. Soc. Lond. A* **460** 2845–64
- [15] Van Gorp A, Bigerelle M and Najjar D 2016 *Polym. Eng. Sci.* **56** 103–17
- [16] Bigerelle M 1999 *PhD Thesis* Ecole Nationale Supérieure d'Arts et Métiers, Lille, France
- [17] Valencia-Lazcano A A, Alonso-Rasgado T and Bayat A 2013 *J. Mech. Behav. Biomed. Mater* **21** 133–48
- [18] Kyle D J T, Oikonomou A, Hill E and Bayat A 2015 *Biomaterials* **52** 88–102
- [19] Evans N T *et al* 2015 *Acta Biomater.* **13** 159–67
- [20] Barr S, Hill E and Bayat A 2009 *Eplasty* **9** e22